JOURNAL OF MECHANICAL ENGINEERING AND SCIENCES (JMES)
ISSN: 2289-4659 e-ISSN: 2231-8380
VOL. 15, ISSUE 1, 7671 – 7683
DOI: https://doi.org/10.15282/jmes.15.1.2021.05.0605

ORIGINAL ARTICLE

Mechanical properties evaluation for engineering materials utilizing instrumented indentation: Finite element modelling approach

Ahmed F. Elmisteri[1], Farag M. Shuaeib[1], Abdelbaset R. H. Midawi[1,2]

[1] Faculty of Mechanical Engineering, University of Benghazi, Benghazi, Libya
[2] Mechanical and Mechatronic Engineering Department, CAMJ group, University of Waterloo, Waterloo, Canada

ABSTRACT – Instrumented indentation technique gives the possibility to determine the mechanical properties for small specimens and material in service. Several researchers have attempted to evaluate this approach experimentally and investigated the factors that affect it by using different indenter's geometries for different engineering materials. In this work, the instrumented indentation technique was used to evaluate the mechanical properties experimentally and numerically using finite element simulation to understand the contact mechanics between the indenter surface and the substrate for two types of steel alloys namely ASTM516-G70 and AISI1010 steel. Two shapes of indenters, blunt (spherical) and sharp (Vickers) were used. The results were then compared with the experimental results extracted from the instrumented indentation test. The results have demonstrated a good agreement between the experimental and the finite element simulation results with error bound a ±5% for young's modulus and ±7.7% for yield strength. Whereas excellent agreement is observed in the elastic region and the beginning of the plastic region for the true stress-strain curve. Finally, it is to be emphasized that the obtained results are more applicable for the tested materials and further research is recommended to accommodate other materials as well and to confirm the generality of this method.

ARTICLE HISTORY
Received: 24th June 2019
Revised: 05th July 2020
Accepted: 12th Sept 2020

KEYWORDS
Instrumented indentation;
ASTM 516-G70;
finite Element;
yield Strength;
hardness;
spherical indenter

INTRODUCTION

An instrumented indentation test or sometimes called depth-sensing indentation instrument used to obtain mechanical properties such as hardness, Young's modulus, and yield strength by analyzing the load-displacement curve. The instrumented indentation test can be performed on a macro or nano-scale using a variety of indenters geometries and the load-displacement curve will represent the shape of the indenter. In microscale, indentation the hardness test was widely used to determine the effect of surface processing such as hardening or coating for different materials, due to the difficulty of performing another mechanical testing [1]. Instrumented indentation test is relatively new and still under development to be more flexible and trust-worthy in use in the field applications. The elastic-plastic response of materials during the indentation has been extensively investigated in the literature experimentally and theoretically [2-6,20]. Determination of the exact shape of the indenter at the tip is important to measure the mechanical properties such as the hardness and the elastic modulus for indentation depths less than a micro-scale [7].

The finite element method has been used to simulate the conical indentation hardness test of elastoplastic micropolar material by S. Hassan Salehi *et al.* [8] Indentation load-depth curves were obtained, and the elastic modulus was calculated. Results justified and showed that the shapes of the plastic zones depend strongly on both the indenter angle and the ratio of young's modulus to yield strength. Where the yield zone of Aluminum (E/σ_y =157.1) is bigger than the yield zone of silicon (E/σ_y =28.8) [8].

Because of the non-linear nature of the indentation hardness test (elasto-plastic behaviour), it is quite hard to obtain the mechanical properties directly from the experimental load-displacement curve. J. A. Knapp *et al.* [9] attempted to characterize layers and thin films using finite element modelling. The yield strength, Young's modulus, and hardness of the layer material extracted, with an absolute accuracy of at least 20% [9]. Improving the test equipment for instrumented indentation method and consideration to the error sources such as the error due to pile-up or sinking in is a way to make it more accurate. Test procedures and concepts are still demanding to improve the method that was introduced 10 years ago [10], Recently, a good agreement between experimental Nanoindentation hardness test for bulk material and finite element simulation in a two-dimensional (2-D) axisymmetric model, and a three dimensional (3-D) model have been obtained by using finite element analysis [11]. Numerical simulations of pure copper, pure titanium, pure iron, and copper film were obtained using FE simulation. It is found that the result depended greatly on mesh size, indenter radius, and the hardening model used to simulate the indentation test [12]. Also, a finite element model for spherical indentation test for metallic substrates have been developed and the results were found to be relatively in close agreement to experimental data with a very minor effect of Poisson's ratio on the load-displacement curve; however, the polymeric materials was less successful because of the effects of anisotropy strain rate dependence e.g., a viscosity [13]. Continuous instrumented indentation test with the Oliver–Pharr method using Vickers's indenter under load values from (10 to 100 N) was

*CORRESPONDING AUTHOR | A. R. H. Midawi | ✉ amidawi@uwaterloo.ca

performed to determine the mechanical properties of Carbide/aluminum composites. Vickers hardness numbers, determined by the Oliver–Pharr method and by conventional hardness measurement are found to be in good agreement [14]. Chi Chen [25] concluded that the finite element method is an effective tool for simulation of the Nano-indentation test on metallic films and limitations caused by the simplification of models and assumptions not be neglected [15]. Midawi *et al.* use the instrumented indentation method to characterize the mechanical properties of engineering alloys, the focus was mainly on the yield strength [16]. Midawi *et al.* found a good agreement between yield strength obtained from the instrumentation indentation test and yield strength obtained from the tensile test for different engineering materials includeing X80 pipeline steel, 516-G70 high strength steel, IF steel, and several aluminum alloys such as AL5052 and AL6463 [16]. Midawi *et al.* used a nearly flat tip indenter in that study, which has an advantage of the constant area, so the yield strength could be estimated directly from the experimental load-displacement curve [17]. In 2017 Midawi *et al.* developed the technique further to estimate the full stress-strain response utilizing the FE inverse approach [18-19] .Herbert *et al*. proposed a model to accuratly measure the mechincal properties (elastic modulud and yield strength) for alumium alloys (6061-T6) and found that the phyical stress-strain can not be accurtly reproduced [5].

In this study, the finite-element method is adopted to build a solid model for the indentation test using different indenters geometries. The goal is to understand the contact mechanics for two different indenters (Vickers indenter and Spherical indenter) and to evaluate the mechanical properties for two different engineering materials. First, the model will be validated against the experimental results, by comparing the FE load-displacement curves with the experimental curves. Then after model validation, a sensitivity analysis was performed by manipulating some parameters in the FE model such as the boundary conditions and strain hardening exponent to find the effect of these parameters on a load-displacement curve. Then the mechanical properties and the stress-strain curves are generated and compared with experimental values.

METHODS AND MATERIALS

Instrumented indentation hardness or depth-sensing indentation is becoming a popular approach used in contact mechanics applications that require measuring hardness and extract other mechanical properties, such as elastic modulus and yield strength. This is achieved by measuring the indenter penetration depth or displacement ″h″ under the applied force P throughout the testing cycle and continue to record the change of the penetration depth after the load removed (unloading). The output is called the load-displacement curve as shown in Figure 1 and Figure 2, and from the load-displacement curve, the elastic solution can determine the hardness, modulus of elasticity, and other mechanical properties.

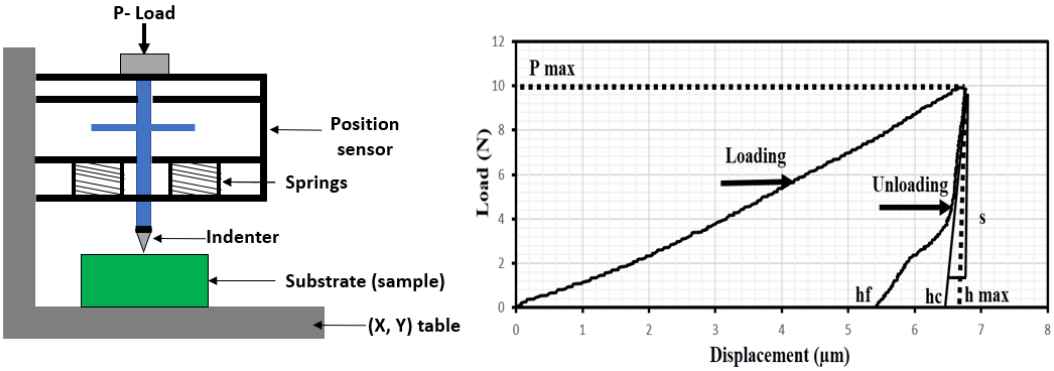

Figure 1. Schematic illustration of an instrumented indentation system

The hardness can be found by dividing the maximum load by the area of contact or projection area, which is determined by the depth of the impression and the known angle or radius of the indenter [20].

$$H = \frac{P_{max}}{A} \tag{1}$$

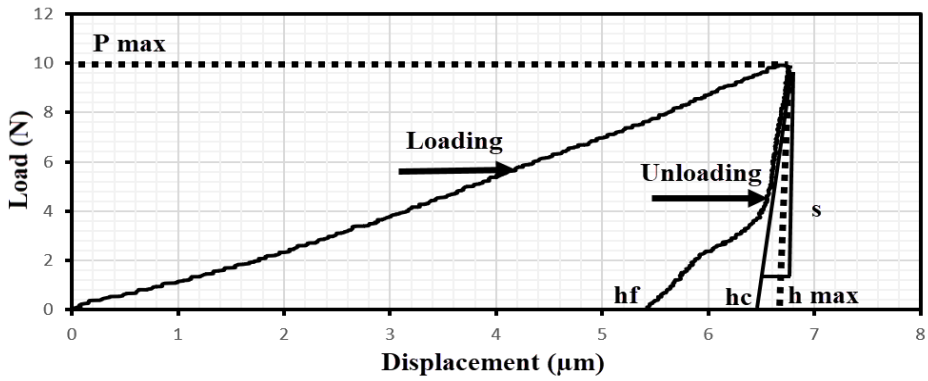

Figure 2. Typical load-displacement curve using spherical indenter

The Oliver–Pharr method was originally developed to measure the hardness and elastic modulus of a single-phase elastic-plastic material from the indentation load-displacement curve with sharp indenters, such as the Berkovich tip. It has been proven that this method can also be applied in any axisymmetric indenter geometries, including a sphere. As shown in Eq. (2) the Oliver–Pharr method begins by fitting the unloading portion of the indentation load-displacement data to the power-law constitutive model [21-22].

$$P = \alpha\,(h - h_f)^m \tag{2}$$

where α and m are the fitting parameters and h_f is the final depth after complete unloading.

The slope of the unloaded curve in Eq. (2) represents the stiffness, and by using it in Eq. (4) the Reduced modulus can be found as follows:

$$S = \frac{d_p}{d_h} \tag{3}$$

$$S = \frac{2}{\sqrt{\pi}}\,E^*\sqrt{A_p} \tag{4}$$

where, A_p is the projection area.

For spherical indenter according to Multiple-point unloading method the projection area equal to:

$$A_p = \pi \times a^2 \tag{5}$$

$$a = \sqrt{2 \times R_i \times h_p} \tag{6}$$

Where:
R_i is the indenter radius.
h_p is the plastic penetration depth.

For Vickers indenter the relationship between the projected area A_p of the indentation and the diagonal diameter d is:

$$A_P = \frac{d^2}{2\,cos\,22} = \frac{d^2}{1.845368} \tag{7}$$

Thus:

$$\frac{d_p}{d_h} = \frac{d}{\gamma}\,E^*\sqrt{\frac{2}{\pi}} \tag{8}$$

where γ is the correction factor equal to 1.0124 for Vickers indenters.

According to Hertz theory, the reduced modulus or the combined modulus of the indenter and the specimen $\mathbf{E}^*$ is given by Eq. (9) as follows:

$$\frac{1}{E^*} = \frac{(1 - v^2)}{E} + \frac{(1 - \grave{v}^2)}{\grave{E}} \tag{9}$$

where, È and $\dot{v}$ are the elastic modulus and Poisson's ratio of the indenter and E and v are the elastic modulus and Poisson's ratio of the specimen. At this stage, the determination of the modulus of elasticity for the specimen is possible as shown in Eq. (10).

$$E = E^* \times (1 - v^2) \tag{10}$$

where, $\frac{(1-\dot{v}^2)}{\dot{E}}$ is too small because the indenter is rigid (means È has large value).

To extract the stress-strain curve from the load-displacement curve by the configuration of the constraint factors, which connect between the normal stress-strain and indentation stress-strain as shown [23]:

$$\sigma_{eff} = \frac{\sigma_{ind}}{\psi} \tag{11}$$

$$\varepsilon_{eff} = \beta \times \varepsilon_{ind} \tag{12}$$

where ψ is the stress constraint factor and β is the strain constraint factor and their value depends on the material. According to recently published work by V.Karthik et al. and also the study conducted by Chao Chang, the values of stress and strain constraint factor for steel are still under investigation and fluctuating between 0.11 to 0.2 for strain constraint factor and 2.87 to 4.1 for stress constraint factor see these articles for more details [24,26,28].

The curve of the indentation stress-strain obtained using the FE model. As shown in Figure 3 there are three distinguishable regimes [25]:

1) An initial elastic regime where the indentation stress evolves linearly with the indentation strain.
2) An elastic-plastic transition regime that exhibits apparent strain hardening attributed to the transformation of the indentation zone from being dominated by elasticity to one dominated by plasticity.
3) A post-yield regime exhibiting the expected perfectly plastic response.

As shown in Eq. (13) the indentation stress equal to the indentation applied load divided by the contact or project area presented in Eq. (5).

$$\sigma_{ind} = \frac{P}{A_P} \tag{13}$$

According to Oliver –Pharr's method, the radius of contact a for spherical indenter calculates from the following Eq. (14).

$$a = \sqrt{2 \times R_i \left(h - \frac{0.75 \times P}{S}\right) - (h - \frac{0.75 \times P}{S})} \tag{14}$$

where h is the penetration depth.

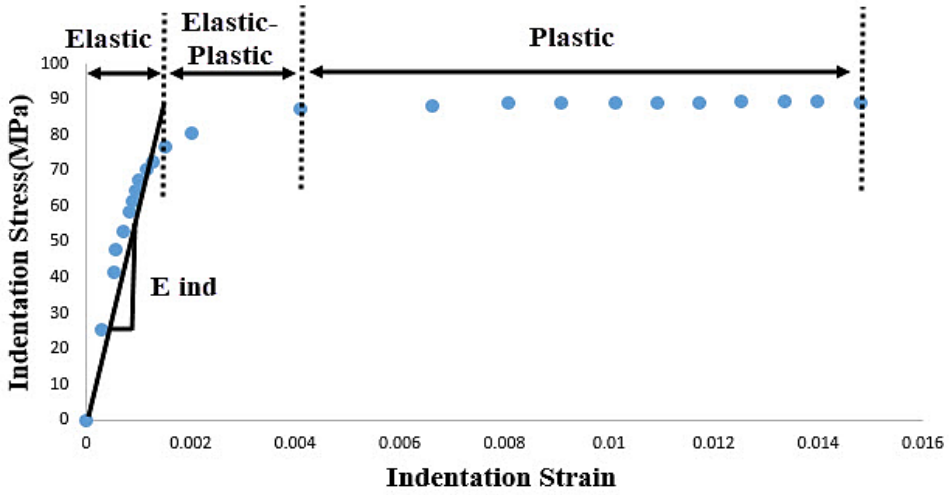

Figure 3. Finite element generated indentation stress-strain curve for soft material

Also, Tabor defines the indentation strain as [20]:

$$\varepsilon_{ind} = 0.2 \frac{a}{R_i} \tag{15}$$

Table 1. Constraint factors for different materials [19]

Materials	E (GPa)	n	E/σ_y	ψ	β
Iron	211	0.26	2970.9	3.81	0.141
Steel	210	0.1	420	4.1	0.105
Steel1	211	0.12	378.33	4.05	0.11
SUS304	196	0.27	965.517	3.7 3	0.138
Aluminum	70	0.295	5622	3.71	0.131
Al7039OA	71	0.115	265.6	4.05	0.11
Cu-51100	113.69	0.076	256.6	4.11	0.091
Cu-10200	110.24	0.305	3991.31	3.52	0.158
Cu-17510	124.02	0.11	204.26	4.01	0.101
Cu20	110	0.485	25217	3.23	0.131
Cu5.3	125	0.52	28115	3.06	0.152
Au	82	0.25	2050	3.82	0.139
Inconel	170	0.293	646.39	3.80	0.146
A5051	73	0.126	948.05	4.01	0.122
Brass	96	0.36	1633.8	3.51	0.154

EXPERIMENTAL SETUP AND FINITE ELEMENT SIMULATION

Materials and Experimental Test

Two widely used steel alloys were investigated in this study AISI 1010 and ASTM 516-G70. These materials were chosen as they are very popular in many industrial applications such as the oil and gas industry and electrical power stations. The main equipment made from these materials includes heat exchangers and pressure vessels see Figure 4. The mechanical properties of these materials are as shown in Table 2. These values were obtained experimentally from the tensile test. The tensile specimens were prepared according to ASTM E8/E8M. The gauge length is sub-size 25mm and the thickness was 1mm [27].

Figure 4. Low-pressure heat recovery steam generation tank in North Benghazi power station used high strength steel alloy ASTM A516-70

The indentation test experiment was performed using the Nanovea mechanical testers, at a maximum load of 10N for spherical indentation and 4N for Vickers indentation. The loading and unloading rate was set at 20N/min for spherical indentation and 8N/min for Vickers indentation, while the approach speed was set to 20μm/min, which corresponds to the speed at which the indenter moves from its starting point towards the sample. Once the sample contacts surface, the

displacement and force were reset to zero The unloading curves were used to derive the modulus values by the analytical technique developed by Oliver and Pharr.

Table 2. Mechanical properties of the considered materials

Materials	Young's modulus E (GPa)	Yield strength σ_y	Poisson's ratio
AISI1010	205	220	0.2
ASTM516G70	240	260	0.23

Modelling Procedure

In this model, the indentation test of bulk materials with isotropic elastic and plastic properties was simulated using the ABAQUS finite element (FE) package. Figure 5 and Figure 6 represent the view of the Spherical and Vickers indentation model. Due to the symmetries of both geometry and loading conditions, the present indentation problem can be reduced to an axisymmetric (2-dimensional) model. The specimen is modelled as an axisymmetric geometry with four-node axisymmetric quadrilateral continuum elements with reduced integration (CAX4R in ABAQUS). Since the indenter is much stiffer than the specimen the indenter is considered to be perfectly rigid and is modelled as an analytical rigid surface. Therefore, there is no need for meshing the indenter [28].

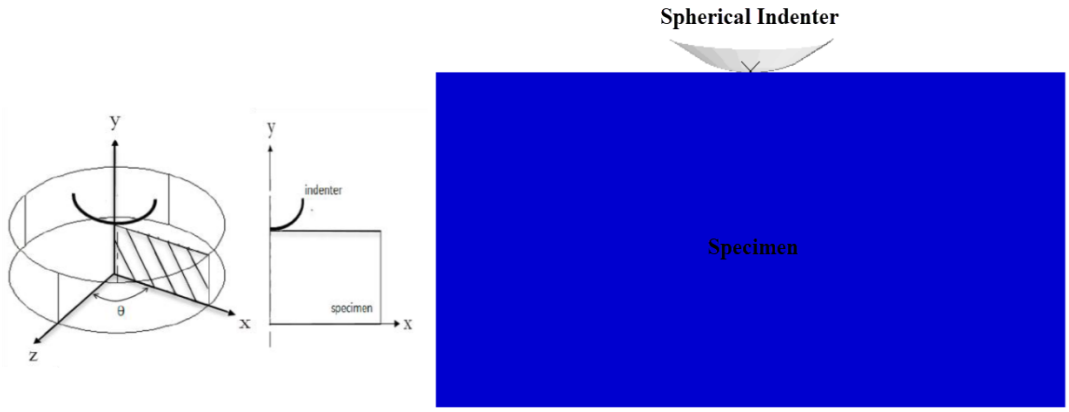

Figure 5. Diagrams show that a 3-D indentation problem can be solved using a 2-D axisymmetric model for Spherical indentation. (adapted from [30])

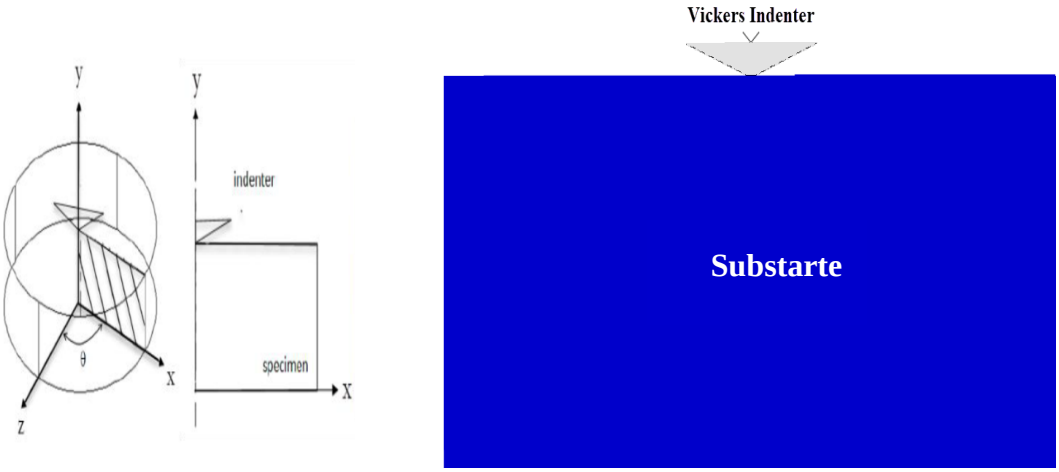

Figure 6. Diagrams show that a 3-D indentation problem can be solved using a 2-D axisymmetric model for Vickers indentation. (adapted from [30])

The specimens are modelled with 38416 four-node axisymmetric reduced integration elements (CAX4R element type) for spherical indentation and 43681 for Vickers indentation. A fine mesh is used around the contact area and near the tip of the indenter. The mesh is continuously coarser further away from the tip, as shown in Figure 7 and Figure 8.

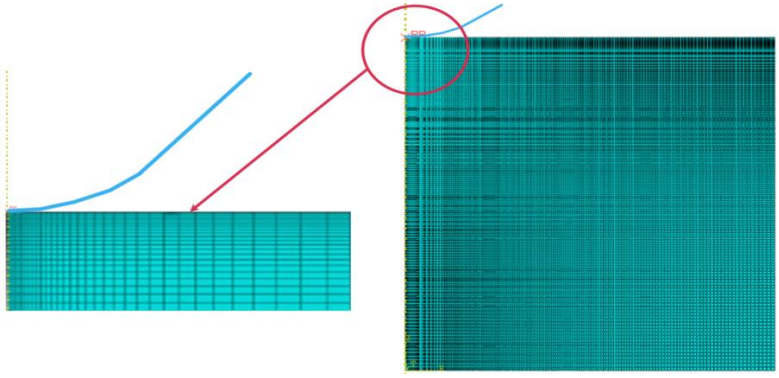

Figure 7. A close look at the mesh detail for spherical indentation (38416 elements)

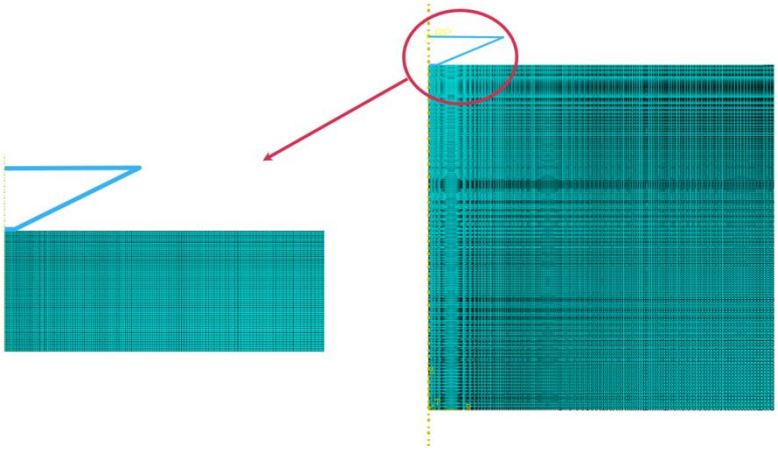

Figure 8. A close look at the mesh detail for Vickers indentation (43681 elements)

The indentation process is simulated both during the loading and unloading steps. During the loading process, the simulation is performed in a displacement control to a depth of equal to the experimental displacement depth in μm in the y-direction (U-2) into the specimen according to the experimental results the depth change depends on the material being indented and the indenter geometry; during the unloading process, the indenter tip returns to the initial position as shown in Figure 9 and Figure 10.

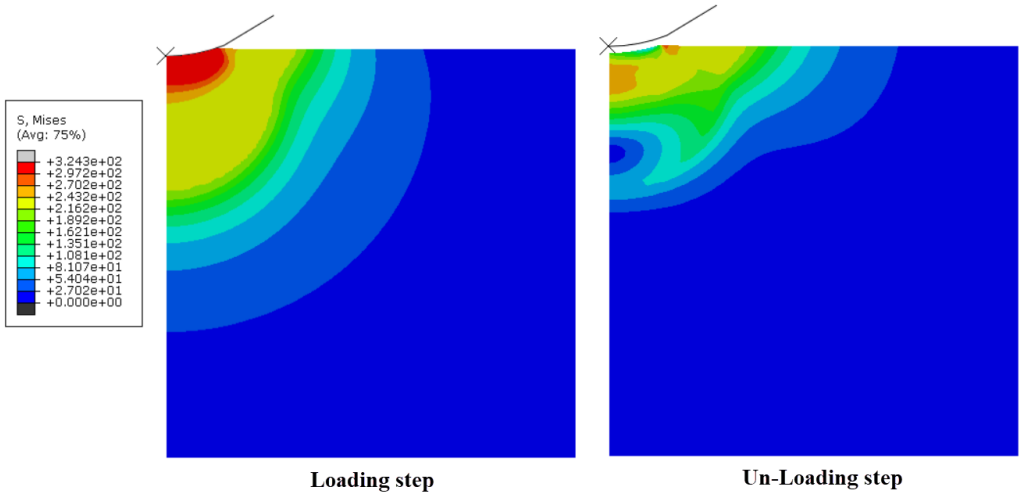

Figure 9. Von-Mises Stress contours represent the loading and unloading contours for AISI-1010 steel using spherical indenter

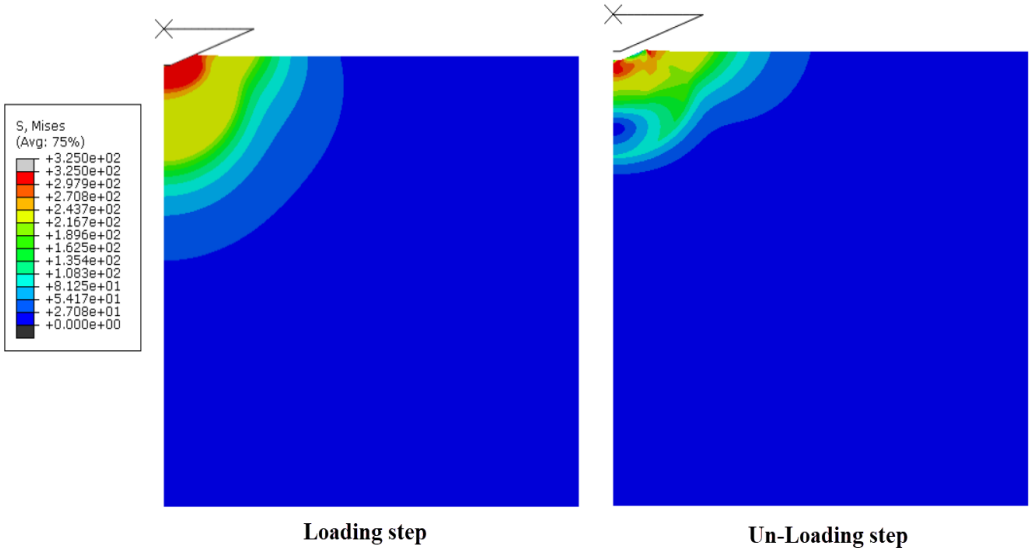

Figure 10. Von-Mises Stress contours represent the loading and unloading contours for AISI-1010 steel using Vickers indenter

The contact constraint is defined by the master and the slave surfaces. Since only the master surface can penetrate the slave surface, the contact direction is then determined by the master surface. The model chooses the indenter as the master surface and the specimen as the slave surface. The boundary conditions are applied along with the original point, centreline, and bottom of the specimen.

The Micro indentation model developed was based on the following assumptions:

- There is a perfect interface between the indenter and the substrate so that the indenter and the substrate will not be separated during the indentation process
- The friction between the indenter tip and the specimen surface is assumed to be zero initially.
- In the calculation, the elastic deformation occurs at the beginning of the process. The specimen starts to deform plastically when the σ_{Mises} reaches to the yield criterion is the yield strength (σ_y).

$$\sigma_{Mises} = \sqrt{\frac{(\sigma_1 - \sigma_2)^2 + (\sigma_2 - \sigma_3)^2 + (\sigma_3 - \sigma_1)^2}{2}} \tag{16}$$

where, σ_1, σ_2 and σ_3 are the three principal stresses. There is no strain hardening behaviour of the specimen considered in the model. The indentation stress and the indentation strain values were obtained directly from the FE model postprocessor routines where the element under the indenter studied is shown in Figure 11.

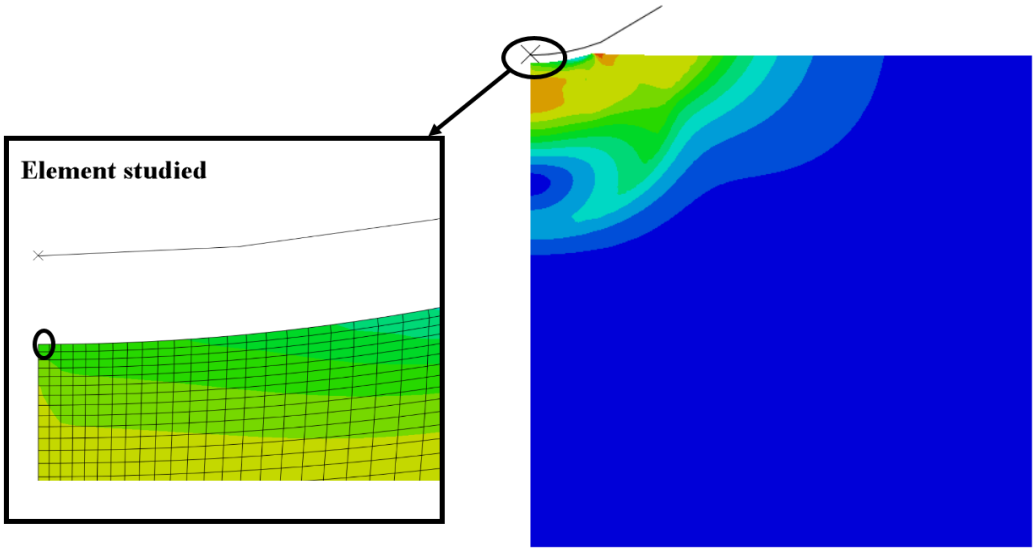

Figure 11. A close look at the contact element

It is found that the engineering stress-strain converted directly from the indentation stress-strain curve of a deep spherical indentation test has agreement with the effective stress-strain value defined by Eqs. (11) and (12). The stress and strain constraint factor has empirical values according to Taber theory and the type of materials as shown in Table 1 above [29].

RESULTS

Model Validation

The indenter used in this experiment was the spherical indenter with 200µm diameter and Vickers indenter with 136^0 between the opposite faces at the vertex. The two commercial steel grades that are widely used in engineering applications are low carbon steel AISI-1010 and ASTM-516-G70 were investigated in this study.

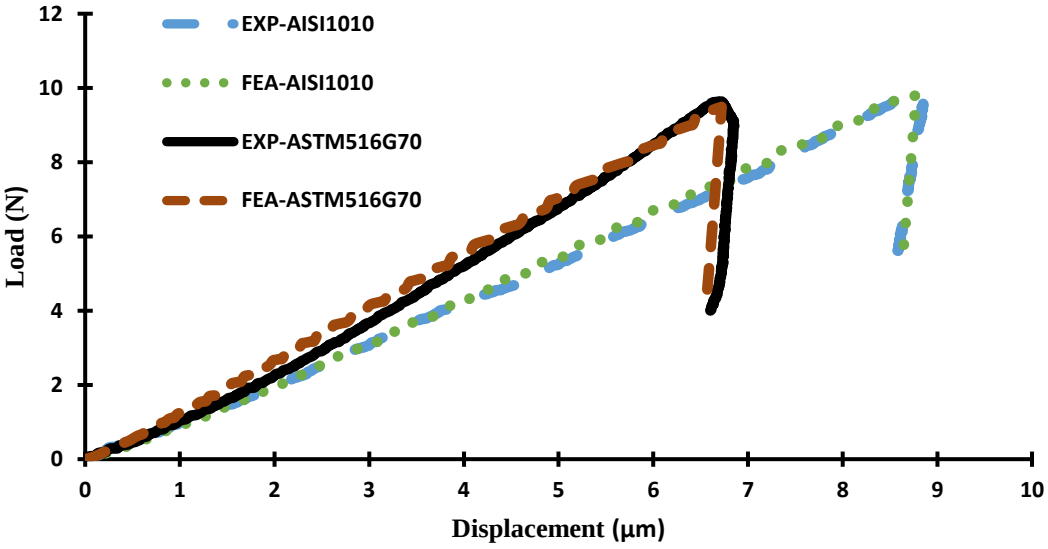

Figure 12. Comparison of F.E simulation and experimental results for spherical indenter

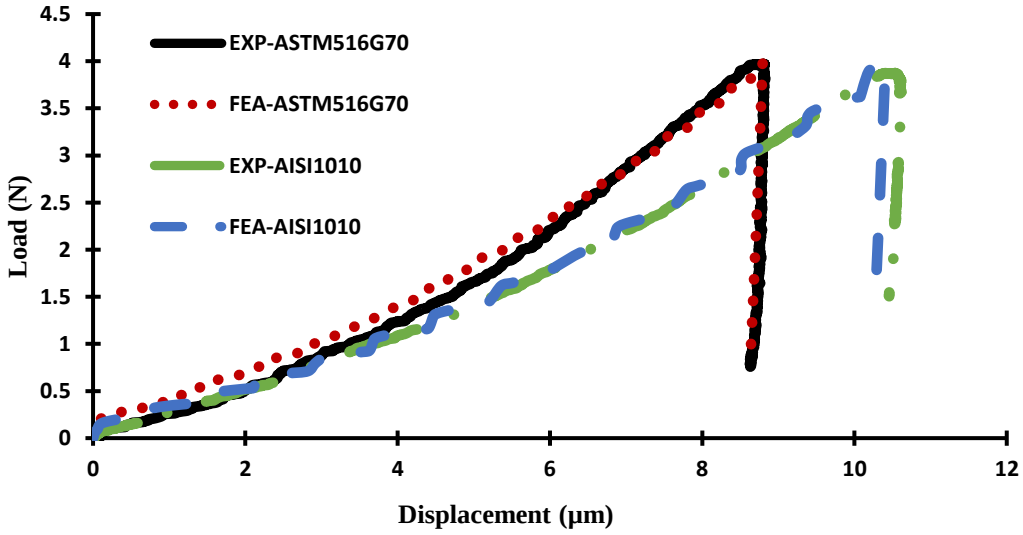

Figure 13. Comparison of F.E simulation and experimental results for Vickers indenter

Figure 12 shows a comparison between the average experimental load-displacement curve and the simulation load-displacement curve for spherical indenter for both AISI1010 and ASTM516G70 materials. Figure 13 shows a comparison between the experimental load-displacement and the simulation load-displacement curves for the Vickers indenter. The agreement between results was excellent for both materials (AISI-1010, ASTM-516-G70), which validate the finite element model. This agreement is found to be sufficient to estimate the yield stress and the strain hardening exponent as

shown in Table 3. Note that the strain hardening exponent values assume that both materials can not be fitted to the same hardening model and that is why showed a higher error.

Table 3. Comparison of yield stress and strain hardening exponent from tensile and indentation tests (Spherical indenter)

Material	Yield Stress (MPa)			Strain hardening exponent		
	Tensile test	Ind. test	Err. (%)	Tensile test	Ind. test	Err. (%)
AISI1010	220	225	2.3	0.149	0.091	38.9
ASTM516-G70	260	280	7.7	0.154	0.139	9.7

Modulus of Elasticity Prediction

Table 4 compares results for elastic modulus extracted from experimental and finite element simulation methods and also from a tensile test. As shown a very good agreement was obtained from the finite element simulation model as compared with other methods and the error percentage (%) is within acceptable limits for both materials.

Table 4. Comparison of modulus of elasticity obtained with different methods for spherical indenter

Material	Modulus of Elasticity (GPa)				
	Typical	Tensile Test (Exp.)	Ind. Test (Exp.)	Ind. Test (FEM)	Error %
AISI-1010	190-210	203	201.6	203.1	0.06
ASTM-516	200-220	240	253.4	252	5.0

Extracted Engineering Stress-Strain Curve

Figures 14 and 15 show the FE simulation results for the stress-strain curve, with the experimental stress-strain curves overlapped on each other for spherical indenter. As shown, there is very good agreement between the experimental engineering stress-strain curve and the effective (FE) stress-strain curve, whereas deviation is observed at the elastic region and the beginning of the plastic part as shown in the effective stress-strain is obtained by selecting 3.7 for stress constraint factor and 0.11 for strain constraint factor for AISI 1010 and 3.9 and 0.11 for ASTM516-G70. These values are according to published data see these articles for more details [26,29].

Suggested that, this deviation comes from the value of stress constraint factor and strain constraint factor, which needs further study, especially studies that tend to change the value of factors according to the nature of the deformation elastic, elastic-plastic, or fully plastic deformation according to Francis [24].

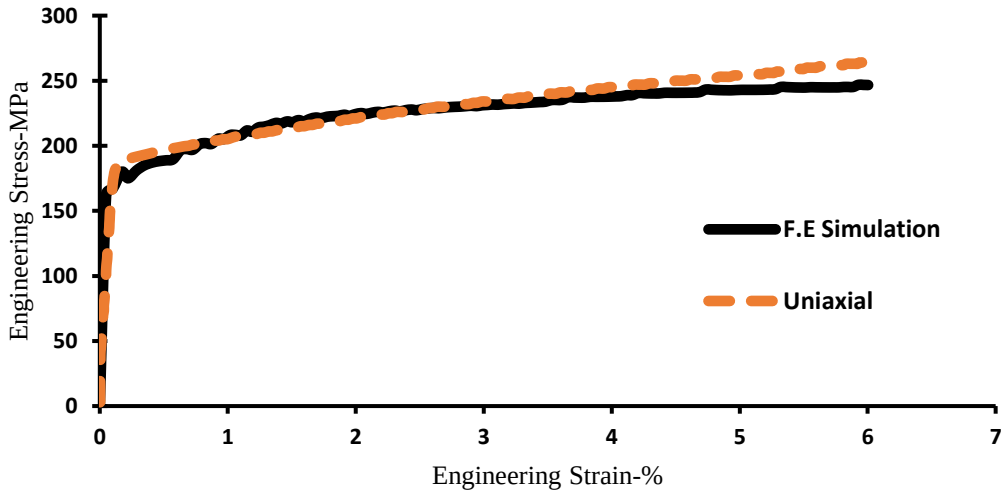

Figure 14. Comparison between F.E simulation and experimental engineering stress-strain curves results for AISI1010

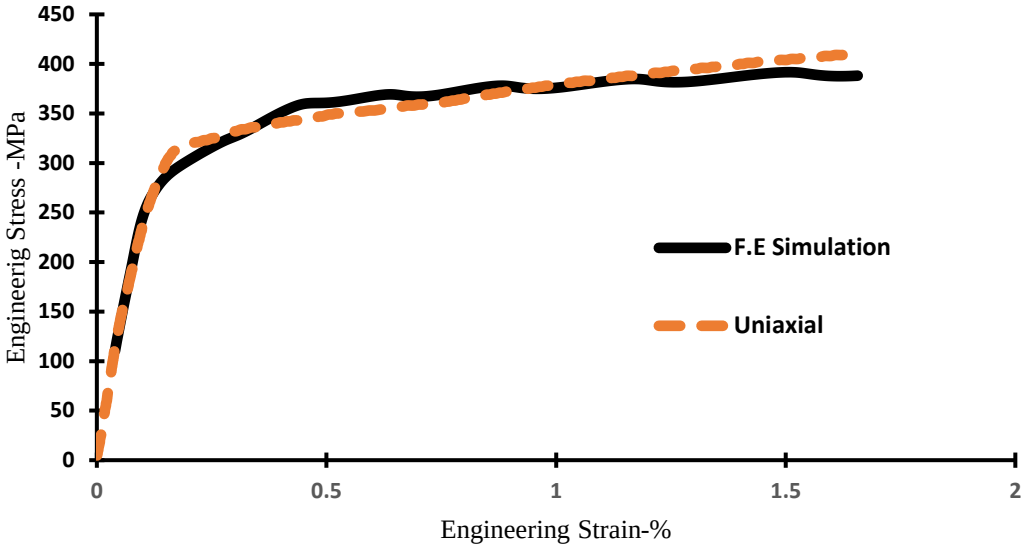

Figure 15. Comparison between F.E simulation and experimental engineering stress-strain curves results for ASTM516-G70

Sensitivity Analysis for the Strain Hardening Exponent Effect

To understand the behaviour of the material under different values of strain hardening (n), Figure 16 shows the indentation loading-unloading curves for the strain hardening indexes of 0.1, 0.2, and 0.3 as assumed values of AISI1010. Accordingly, two points were observed. The first one is, lower indentation load is required to make the same indentation for the material of large strain hardening as expected. The second is, the strain hardening has no significant effect on the slope of the unloading curves at the onset of the unloading. This means that the unloading behaviour is controlled by the elastic properties of materials if there is no change in the microstructure and defects in the materials.

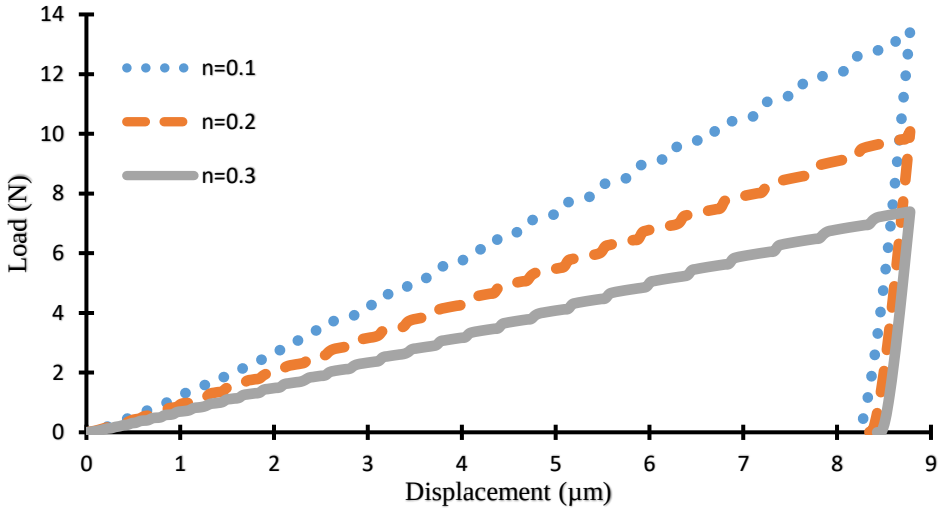

Figure 16. Load- Displacement curve of AISI1010 for different strain hardening exponent (spherical indenter)

CONCLUSION

In conclusion, it is found that finite element simulation has become a powerful tool to study the micro- indentation test and thus to help develop improvements in the analytical theories used to extract mechanical properties from experimental data. In this work, the indentation FE simulation has been implemented in the ABAQUS software based on the material properties obtained from the uniaxial tensile tests of ASTM516G70 and AISI1010 steel. From this study the following points have been concluded:

- The FE simulation is a suitable tool to simulate the instrumented indentation test and extract mechanical properties such as Young's modulus, yield strength, and Strain hardening exponent (n).

- By referring to the selected materials (AISI101, ASTM516G70) the obtained Young's modules error with a maximum of 5% which is an excellent result, and for Yield strength is with a maximum of 7.7% which is also within the acceptable range. More specifically, the Yield strength determination is a significant contribution.
- As an analytical tool, FE simulation helps to lower the cost and safe time of experimental studies, which can be used to understand the contact mechanics and predict the mechanical properties of engineering materials accurately and rapidly.
- Attention should be given to some factors that may affect the FE modelling results when sharp indenters are used such as friction between the indenter surface and the substrate and hardening model used to simulate the material plastic behaviour.
- In future studies, the authors will focus on applying this technique to extract the mechanical properties of coated materials and welded structures to estimate the narrow zones of mechanical behaviour such as the heat-affected zone.

ACKNOWLEDGMENTS

The authors would like to thank Prof. Adrian Gerlich from the University of Waterloo for his support and for giving us access to the instrumented indentation machine at the University of Waterloo, CAMJ lab, Waterloo, ON, Canada.

REFERENCES

[1] M. A. A. Afripin, N. A. Fadil, M. N. Tamin, "Deformation mechanics of sputtered copper layers during nanoindentation tests", *Journal of Mechanical Engineering and Sciences*, vol. 14, no. 1, pp. 6504 – 6513, 2020.

[2] S. S Chiang D.B. Marshall and A.G. Evans, "The response of solids to elastic-plastic indentation", *Journal of Applied Physics*, vol. 53, pp. 298, 1981.

[3] Sung-Hoon Kim, Min-Kyung Baik, Dongil Kwon, "Determination of Precise Indentation Flow Properties of Metallic Materials Through Analyzing Contact Characteristics Beneath Indenter", *Journal of Engineering Materials and Technology*, Vol. 127, pp. 265-272. 2005.

[4] Yanping Cao, Xiuqing Qian, Norbert Huber, "Spherical indentation into elastoplastic materials: Indentation-response based definitions of the representative strain", *Journal of Materials Science and Engineering*, Vol. 454-455, pp. 1-13. 2007.

[5] E.G Herbert, G.M Pharr, W.C Oliver, B.N Lucas, J.L Hay, " On the measurement of stress-strain curves by spherical indentation", Journal of Thin Solid Films, Vol. 398-399, pp. 331-335. 2001.

[6] J.K.Phadiker, T.A. Bogetti, A.M. Karlsson, " On the uniqueness and sensitivity of indentation testing of isotropic materials ", *International Journal of Solids and Structures*, Vol. 50, Issues 20-21, pp. 3242-3253. 2013.

[7] M. F. Doerner and W. D. Nix, "A method for interpreting the data from depth-sensing indentation instruments", *J. Mater. Res.*, vol. 1, no. 04, pp. 601–609, 1986.

[8] A.K. Bhargava, C.P. Sharma, "Mechanical behavior and testing of materials", *PHI Learning Private Limited, Delhi*, 1990; ISBN -978-81-203-4250-7.

[9] J.A. Knapp, "Finite-element modeling of Nanoindentation for determining the mechanical properties of implanted layers and thin films", *Nuclear Instruments and Methods in Physics Research Section B: Beam Interactions with Materials and Atoms*, vol. 127-128, pp. 935-939, 1996.

[10] W.C. Oliver, G.M. Pharr, "An improved technique for determining hardness and elastic modulus using load and displacement sensing indentation experiments", *Materials Research Society*, vol. 7, no. 6, pp. 1564-1583, 1992.

[11] N. Panich, V. Kraivichien, S. Yong, "Finite Element Simulation of Nanoindentation of Bulk Materials", *J. Sci. Res. Chula. Univ.* vol. 29, no. 2, pp. 145-153, 2004.

[12] J.D. Bressan, A. Tramontin, C. Rosa, "Modeling of Nanoindentation of bulk and thin film", *Joinville Department of Mechanical Engineering, Universidad do Estado de Santa Catarina (UDESC)*, Joinville, SC, Brazil, 2004.

[13] D. John. Clayton, "Spherical Indentation in Elastoplastic Materials: Modeling and Simulation", *Army Research Laboratory*.2005; ARL-TR-3516.

[14] E. Kimmari and L. Kommel, "Application of the continuous indentation test method for the characterization of mechanical properties of B4C/Al composites", *Proceedings of the Estonian Academy of Sciences*, vol. 12, no. 4, pp. 399-407, 2006.

[15] C. Chen, "2-D finite element modeling for Nanoindentation and fracture stress", *Graduate Theses and Dissertations*, 2009, DOI:http://scholarcommons.usf.edu/etd/1897.

[16] A.R. H. Midawi Y. Kisaka, E.B.F. Santos, A.P. Gerlich, "Characterization of local mechanical properties of X80 pipeline steel welds using advanced techniques Paper", *The American Society of Mechanical Engineers (ASME)*, pp. V003T05A042, 8 page, 2016. DOI:10.1115/IPC2016-64238.

[17] A. R. H. Midawi, C.H.M. Simha, A.P. Gerlich, "Novel techniques for estimating yield strength from loads measured using nearly-flat instrumented indenters", *Materials Science and Engineering A*, vol. 675, pp. 449-453, 2016.

[18] A.R.H. Midawi, C.H.M. Simha, M.A. Gesing, A.P. Gerlich, " Elastic-plastic property evaluation using a nearly flat instrumented indenter ", *International Journal of Solids and Structures*, Vol. 104-105, pp.81-91. 2017.

[19] A.R.H. Midawi, " Evaluation of Mechanical Properties in Pipeline Girth Welds Using Instrumented Indentation ", *University of Waterloo, Waterloo, ON, Canada*, 2018.

[20] A. C. Fischer, *Cripps*, "Mechanical Engineering Series Nanoindentation", *Springer Science and Business Media*, New York, 2002. DOI 10.1007/978-0-387-22462-6.

[21] W. C. Oliver, "Measurement of hardness and elastic modulus by instrumented indentation: Advances in understanding and refinements to methodology", *Journal of Materials Research*, vol.19, pp. 3-20, 2003.

[22] Q. Kan, W. Yan, G. Kang, Q. Sun, O. Phar, "Indentation method in determining elastic moduli of shape memory alloys—A phase transformable material", *Journal of the Mechanics and Physics of Solids*, vol. 61, pp. 2015-2033, 2013.

[23] D. Tabor, *Hardness of Metals*, Clarendon, Oxford, UK,1951.

[24] V. Karthik, K. V. Kasiviswanathan, B. Raj, "Miniaturized testing of engineering materials", *CRC Press*, Sound Parkway NW, 2017.

[25] D. K. Patel and S. R. Kalidindi, "Correlation of spherical Nanoindentation stress-strain curves to simple compression stress-strain curves for elastic-plastic isotropic materials using finite element models", *Acta Materialia*, vol. 112, pp. 295-302, 2016.

[26] B. Xu and X. Chen, "Determining the engineering stress-strain curve directly from the load–depth curve of spherical indentation test", *Journal of Materials Research*, vol. 25, pp. 2297-2307, 2010.

[27] Standard Test Methods for Tension Testing of Metallic Materials, *ASTM International*, West Conshohocken, PA, 2013

[28] ABAQUS Version 6.14 User's Manual, Providence, Rhode Island, 2018.

[29] C. Chang, M. A. Garrido, J. Ruiz-Hervias, Z. Zhang, L. Zhang, " Representative Stress-Strain Curve by Spherical Indentation on Elastic-Plastic Materials", *Advances in Materials Science and Engineering*, vol. 2018, pp. 1-9, 2018.

[30] J. Joseph, *Numerical Modeling and Characterization of Vertically Aligned Carbon Nanotube Arrays*, 2013, Theses and Dissertations--Mechanical Engineering, 2013.